ACS Energy LETTERS

Cite This: ACS Energy Lett. 2018, 3, 184−190

# Transforming Two-Dimensional Boron Carbide into Boron and Chlorine Dual-Doped Carbon Nanotubes by Chlorination for Efficient Oxygen Reduction

Zongkui Kou,[†] Beibei Guo,[†] Daping He,[†,‡] Jian Zhang,[†] and Shichun Mu*[,†]

[†]State Key Laboratory of Advanced Technology for Materials Synthesis and Processing, Wuhan University of Technology, Wuhan 430070, People's Republic of China

[‡]Hubei Engineering Research Center of RF-Microwave Technology and Application, Wuhan University of Technology, Wuhan 430070, China

Supporting Information

**ABSTRACT:** **Our theoretical calculations suggest that the synergistic effect between the electron acceptor (B) and donor (Cl) in carbon nanotubes (CNTs) (BClCNTs) is the key to excellent oxygen reduction reaction (ORR) activity. However, the rational fabrication of BClCNTs is still an open question. Here, we first present a metal-free and controlled strategy for successful preparation of BClCNTs via chemically tailoring two-dimensional (2D) boron carbide ($B_4C$) with $Cl_2$. Accompanied by partial extraction of B atoms from $B_4C$ with $Cl_2$, the residue B and C atoms combining with Cl atoms self-organize into nanotube microstructures. Significantly, the amount of heteroatoms (B and Cl) can be tuned in terms of altering chlorine-to-carbide molar ratios. As expected, as a metal-free ORR catalyst, the produced BClCNTs exhibit a higher onset potential (0.94 V vs a reversible hydrogen electrode; RHE) and half-wave potential (0.84 V) as well as greater stability than those of commercial Pt/C (0.92 and 0.80 V).**

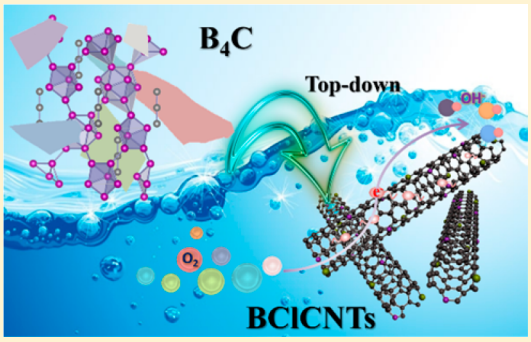


Since carbon nanotubes (CNTs) were first obtained by arc-discharge,[1] they have undoubtedly become one of the hot topics in nanotechnology due to excellent properties that contribute to diverse applications. For instance, they have plenty of $\pi$ electrons,[2] leading to wide applications for reactions needing electrons, such as the oxygen reduction reaction (ORR).[3−6] Unfortunately, due to the inertness of these electrons, they cannot be directly used. Recently, it has been revealed that heteroatom (such as N, S, P) doped CNTs (HDCNTs) can tune their bandgap and thus efficiently activate inert $\pi$ electrons.[7−9] Although some work has been done in different ways regarding endohedral doping, the case of substitutional doping has still some difficulties to overcome.[10−12]

Therefore, developing a simple but efficient strategy for such HDCNTs is significant. Until now, useful preparation methods reported mostly focus on chemical vapor deposition (CVD),[2] pyrolysis,[13] electrolysis,[14] and template methods.[15] Among them, the CVD method has received plenty of attention due to well-regulated size, alignment, and heteroatomic configurations of as-received CNTs.[8] Through a thermal CVD method, Dai et al. fabricated vertically aligned B and N dual-doped CNTs and exploited possible synergetic effects of co-doping with B and N on ORR activities.[12] However, traditional CVD processes have suffered from multiple steps, high cost, and operational complexity.[2,8−11] Recently, metal−organic frameworks (MOFs) were used as a solid carbon source to grow HDCNTs.[16−18] For example, Lou et al. reported a dual-MOF confined-pyrolysis approach for the preparation of iron carbide nanoparticle-embedded CNT assemblies.[19] More recently, HDCNTs can be derived from prevailed biomass materials. Zhao et al. used a solid biomass carbon source to obtain O-doped CNTs.[20] Nevertheless, these HDCNTs obtained by the above methods suffered from uncontrollable doping configurations due to use of nanocatalysts and high-temperature pyrolysis.

Our density functional theory (DFT) calculations suggest the synergistic effect between electron acceptor (B) and

Received: November 16, 2017
Accepted: December 20, 2017
Published: December 20, 2017

  

DOI: 10.1021/acsenergylett.7b01133
ACS Energy Lett. 2018, 3, 184−190

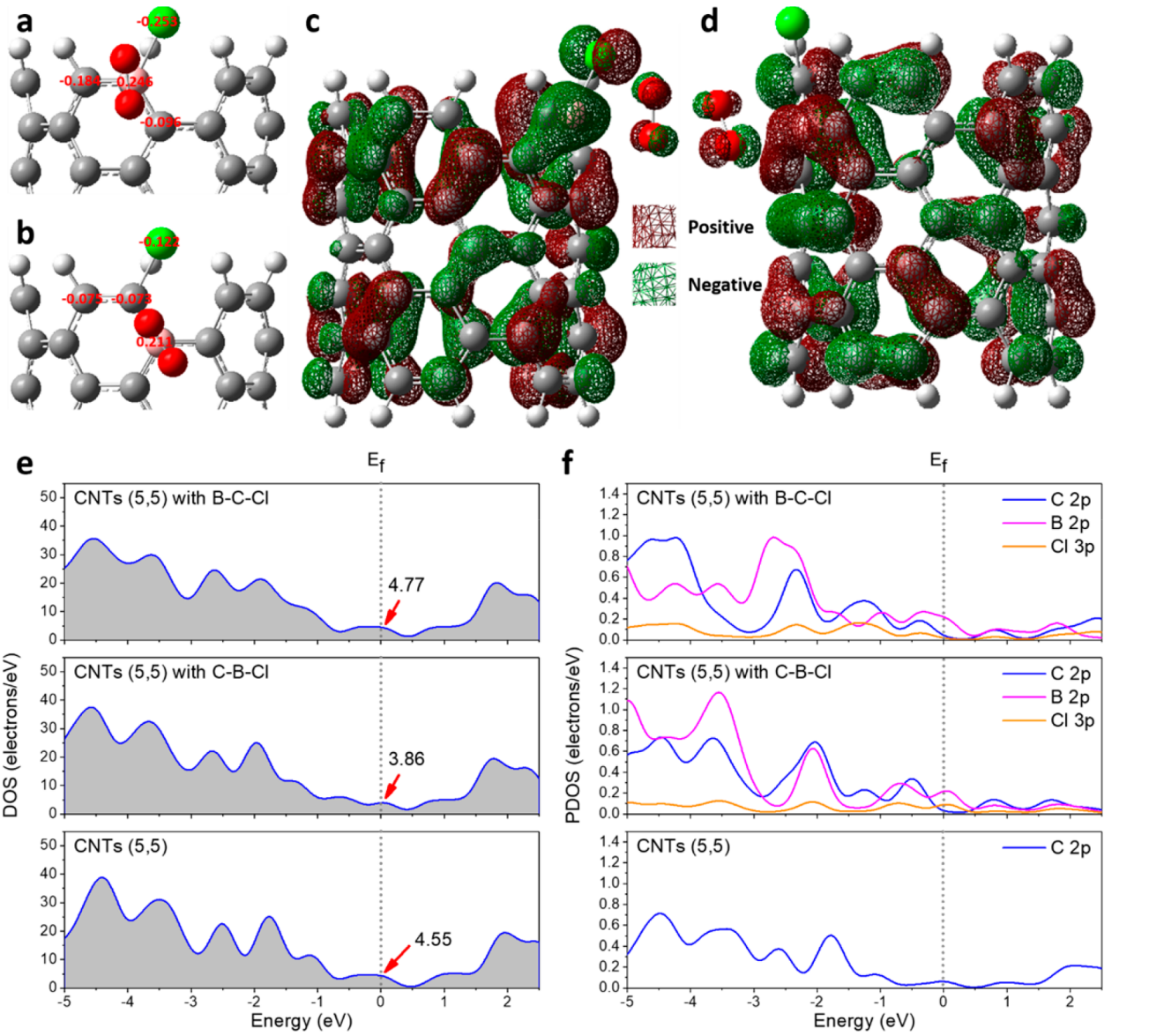


**Figure 1. (a,b) NBO charges for atoms near the doping atoms of BClCNTs(5,5) with C−B−Cl (a) and B−C−Cl (b) moieties. (c,d) HOMO plots of the corresponding $O_2$ adsorption configuration (isodensity value of 0.007 au). H, gray; B, pink; C, pink; O, red; Cl, green. (e,f) DOS (e) and PDOS (f) of pristine CNTs(5,5) and CNTs(5,5) with a C−B−Cl or B−C−Cl moiety.**

electron donor (Cl) atoms in the B and Cl dual-doped CNTs (BClCNTs) toward enhancing ORR activity, but there is no report on successful fabrication of BClCNTs. By a simple chlorination method, Yury and co-workers have converted plenty of carbides into various porous carbide-derived carbon (CDC) nanomaterials.[21] Recently, by partially chloridizing carbides, we converted 2D metal carbides into various homologous metal-doped graphene.[22] Here we first find that this strategy can also be used to directly synthesize BClCNTs via chemically tailoring 2D $B_4C$ nanoflakes with $Cl_2$. Followed by partial extraction of B atoms from $B_4C$ with $Cl_2$, the B, C, and Cl atoms in the system can self-organize into a tubular microstructure. Such a chemical reaction process allows the produced BClCNTs with adjusted B and Cl doping configurations. Electrochemical measurements are also used to testify to the high ORR activity of BClCNTs.

Electron acceptor and donor co-doping into carbon nanomaterials can synergistically activate $\pi$ electrons in the $sp^2$ carbon for use in ORR and thus has attracted wide attention.[2,7,9,12] Here we first started with first-principle DFT calculations to unveil the possible synergetic effects of the electron acceptor (B) and donor (Cl) in the heteroatom-doped CNTs for ORR. The role of two possible co-doping configurations (C−B−Cl and B−C−Cl moieties, namely, bonded and separated boron and chlorine) in the armchair (5,5) single-walled CNT (CNT(5,5)) was modeled and investigated as active centers toward ORR by DFT calculations before and after $O_2$ adsorption, including geometry optimization and subsequent natural bond orbital (NBO) analysis.[7] In the optimized structures, the substitutional boron atom is three-coordinate ($BC_3$) and exhibits $sp^2$-like hybridization in B−C $\sigma$ bonds while the Cl atom as an sp-like hybridization with a C atom (Cl−C) is located in the edge of CNTs (Figure S1 and Table S1). For a pure CNT(5,5), it is always electrically neutral (Figure S2a). However, after Cl-doping into CNT(5,5) (ClCNTs(5,5)), the neighboring carbon atom is positively charged with a value of 0.016 (Figure S2b), which is favorable for capture of the $O_2$ molecule.[23] When the B atom is further



DOI: 10.1021/acsenergylett.7b01133
ACS Energy Lett. 2018, 3, 184−190

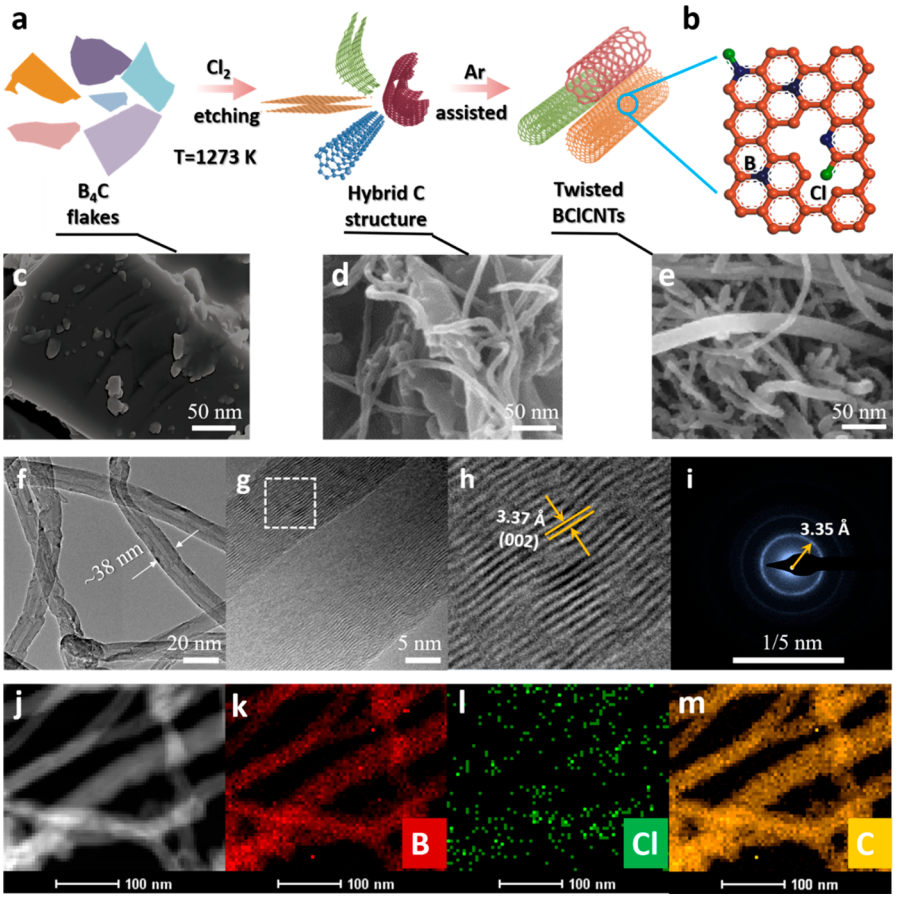


**Figure 2. (a) Schematic illumination of one-step evolution from $B_4C$ to BClCNTs. (b) Possible locations for B and Cl co-incorporation into CNTs. (c–e) SEM images of the pristine $B_4C$ nanoflakes (c), transitional hybrid carbon structure (d), and the resultant BClCNTs (e). Low-magnified and (f) high-magnified TEM (g) and its intercepted part (h) and SAED images (i) of the as-synthesized BClCNTs. (j) STEM-HAADF images of the typical BClCNTs. (k–m) HAADF intensity mapping: boron mapping (k), chlorine mapping (l), and carbon mapping (m).**

introduced into ClCNT(5,5), it induces quite an amount (0.255 and 0.209) of positive charge on the B atom of BClCNTs with C–B–Cl and B–C–Cl moieties, respectively (Figure 1a,b). This positively charged boron atom is favorable for capture of the $O_2$ molecule, which is slightly negatively charged upon approaching the tube.

Importantly, the results show that for the BClCNT(5,5) with a C–B–Cl moiety (Figure 1c), the adsorbed $O_2$ keeps the same bond length (1.21 Å) as the gaseous $O_2$ (Table S2), indicating a physisorption mode. However, CNT(5,5) with a B–C–Cl moiety (Figure 1d) presents more exacted charges of 0.081 electrons per oxygen molecule (this value is only 0.001 for the C–B–Cl), and the O–O band distance increases to 1.28 Å (Table S2), demonstrating that the $O_2$ molecule is strongly chemically bonded to CNTs.[24] Moreover, the introduction of the B–C–Cl moiety lifts the highest-occupied molecular orbitals (HOMOs) by 0.05 eV and reduces the HOMO – lowest unoccupied molecular orbital (LUMO) gap by 0.17 eV compared with C–B–Cl moiety (Figure S3), suggesting easy transfer of the electron from the nanotube to the adsorbed oxygen. This indicates that the B–C–Cl moiety plays a more positive role in promoting the ORR process. According to Khalfoun's calculations, the localized transport phenomena for isolated B or N doping are recovered when B and N atoms are far apart in the dual-doped CNTs.[25] In essence, the chlorine can act with the same effect as nitrogen due to its higher electronegativity than that of carbon.

Additionally, we have calculated the density of states (DOS) and partial DOS (PDOS) of three models (details of calculations are presented in the Supporting Information). As shown in Figure 1e, the DOS of perfect CNT(5,5) shows it to be metallic with a conductive band crossing the Fermi level. The incorporation of the C–B–Cl domain into CNTs leads to a decreasing DOS value at the Fermi level, whereas the B–C–Cl domain can increase the DOS value. Therefore, B–C–Cl can more effectively activate the electronic structure of CNTs. The PDOS analysis (Figure 1f) for perfect CNTs(5,5) shows that the C 2p contributes major electronic states in the vicinity of the Fermi level. For the CNTs(5,5) with C–B–Cl and B–C–Cl, both B and C 2p orbitals are very high lying states with major contributions toward the PDOS. Remarkably, for the CNTs(5,5) with B–C–Cl, in the conduction band region, B 2p orbitals have more contribution in comparison with the other two models. Therefore, the co-introduction of B and Cl into a CNT as the B–C–Cl domain can keep the robust capability of conjugating with the carbon $\pi$ electrons, which is predicted to be significantly active for ORR.[2]

From the results of DFT calculations, BClCNTs present an enhancing ORR activity over undoped CNTs and ClCNTs owing to the synergistic role of doping B and Cl atoms. However, facile synthesis of BClCNTs is difficultly imple-



DOI: 10.1021/acsenergylett.7b01133
ACS Energy Lett. 2018, 3, 184–190

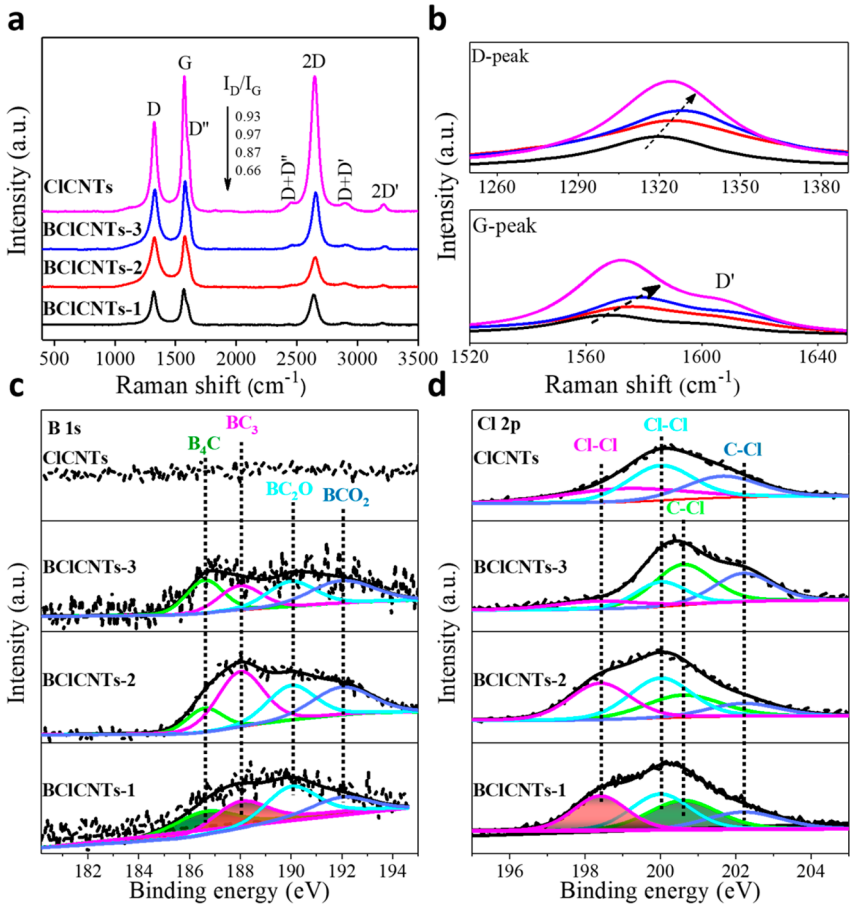


**Figure 3. (a) Raman spectra (632.8 nm laser wavelength) of BClCNTs and ClCNTs. (b) Magnified images of the D-peak and G-peak corresponding to (a). (c,d) Typical XPS spectra of B 1s (c) and Cl 2p (d).**

mented. In this work, after removing partial B atoms from $B_4C$ with insufficient chlorination, we find that the B, C, and Cl atoms in the system can self-organize and gradually roll into BClCNTs with the aid of Ar gas at a high temperature of 1273 K (Figure 2a). In the produced BClCNTs, possible locations of B and Cl atoms are present in Figure 2b. Such a classic chemical tailoring process was first investigated by electron microscope images. As shown in Figures 2c and S4, the pristine $B_4C$ presents a 2D nanoflake morphology. Powder X-ray diffraction patterns (PXRD, Figure S5) show that pristine $B_4C$ nanoflakes are perfect monocrystals (PDF 35-0798 of hexagonal $B_4C$). Rhyming with the extraction of B atoms by $Cl_2$ (Figure S6), the remaining atoms in the system gradually self-organize and roll up (Figure 2d) and finally evolve into BClCNTs (Figures 2e and S7). Such a nanotube has a typical diameter of ~38 nm (Figure 2f) and a multiwall microstructure (Figure 2g) with a interplanar spacing of 3.37 Å assigned to C(002) (Figure 2h). The selected area electron diffraction (SAED) image (Figure 2i) shows a diffraction ring with a diameter of 3.35 Å, indicating a random orientation of nanotubes. Apparent morphological differences of the BClCNTs are observed in comparison with pristine $B_4C$ nanoflakes (Figure S8), suggesting successful conversion between them. We also find that B atoms can thoroughly react with $Cl_2$, leading to the formation of Cl-doped CNTs (ClCNTs) (see the elemental analysis of Table S3). All of the products including BClCNTs-$x$ ($x$ = 1, 2, 3) and ClCNTs obtained with an increasing chlorine-to-carbide molar ratio ($\chi$, Figure S9) present a similar tubular microstructure with twist features, which demonstrates that the enhanced $\chi$ cannot influence the morphology of the products.

To check the atomic distribution of B and Cl across the typical BClCNTs, we conducted high-angle aberration-corrected dark-field scanning transmission electron microscopy (STEM-HAADF) imaging by an aberration-corrected STEM (Figure 2j). It can be found that B atoms (Figure 2k) and C atoms (Figure 2m) in BClCNTs jointly construct tubular networks, suggesting possible B−C six-membered rings (Figure 2b). However, Cl atoms (Figure 2l) are scattered outside of the nanotubes.

In Raman spectra, the characteristic peaks at 477, 528, 729, 792, and 1068 cm$^{-1}$ without representative D- and G-bands of carbon-based materials (Figure S10) demonstrate the high purity of $B_4C$ precursors.[26] For nanotubes, the intensity of all of the peaks (Figure 3a) gradually increases, which suggests an evolution into more complete tubular microstructures.[27] D and G peaks (Figure 3b) blue shift with increased $\chi$, which is due to the decreased doping atoms in quantity (Table S3). The intensity ratio of D- and G-bands ($I_D/I_G$) is a powerful value to evaluate defects in the carbon nanomaterials.[27] Among all of the products, BClCNTs-2 has the highest $I_D/I_G$ value, indicating the presence of most defects that are conducive to electrocatalytic processes.[9]

X-ray photoelectron spectroscopy (XPS) spectra (Figure S11) further uncover the existence of B and Cl atoms in BClCNTs. High-magnified XPS was conducted to characterize



DOI: 10.1021/acsenergylett.7b01133
ACS Energy Lett. 2018, 3, 184−190

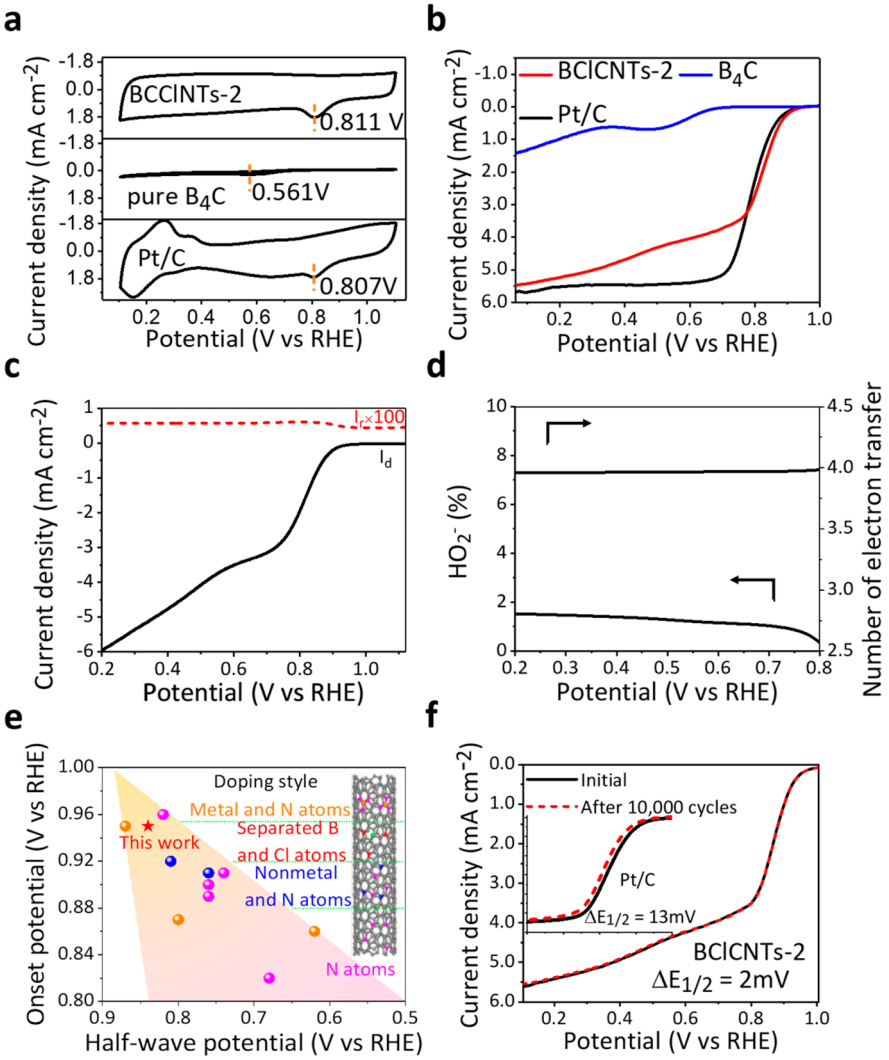


**Figure 4. (a) CVs in oxygen-saturated 0.1 M KOH at a scan rate of 50 mV $s^{-1}$. (b) RDE voltammograms in oxygen-saturated 0.1 M KOH at various electrodes. (c) RRDE tests (1600 rpm) of the optimal BClCNTs-2 for ORR in 0.1 M KOH saturated with oxygen at a scan rate of 5 mV $s^{-1}$. (d) Percentage of peroxide and the number of electron transfers based on the RRDE result. (e) Volcano plots of the onset potential as a function of the half-wave potential for HFCNTs-based ORR electrocatalysts. (f) RDE polarization curves of the studied catalyst and Pt/C (inset figure) before and after 10000 potential cycles in $O_2$-saturated 0.1 M KOH.**

the configurations of the B (Figure 3c) and Cl (Figure 3d) elements in the samples. The spectra of both B 1s and Cl 2p display four characteristic peaks indicating the diverse chemical states of B and Cl dopants. B1 (186.6 eV) and B2 (188.0 eV) peaks in the B 1s spectrum correspond to $B_4C$ and $BC_3$ in the nanotubes,[28] respectively. Another two peaks in the B 1s spectrum correspond to $BC_2O$ and $BCO_2$ moieties.[29] For the Cl 2p spectrum, the two peaks (198.4 and 200.2 eV) are assigned to Cl−Cl,[30] while another two peaks (200.6 and 202.2 eV) belong to C−Cl.[31]

The ORR performance of the as-synthesized BClCNTs is evaluated using a rotating disk electrode (RDE) technique. Cyclic voltammetry (CV) curves clearly reveal oxygen reduction peaks for all investigated samples in an $O_2$-saturated 0.1 M KOH solution (Figure 4a). The resultant BClCNTs-2 exhibits a most striking ORR peak at 0.811 V vs a reversible hydrogen electrode (RHE) against the $B_4C$ precursor (0.561 V) and the commercial Pt/C (0.807 V). We also conducted linear scan voltammogram (LSV) tests to evaluate the potential of BClCNTs for ORR. The excellent ORR performance is also obtained by comparing the onset potential ($E_{onset}$ = 0.94 V vs RHE) and half-wave potential ($E_{1/2}$ = 0.84 V vs RHE) in the RDE polarization curves (Figure 4b), which are higher than those of commercial Pt/C ($E_{onset}$ = 0.92 V; $E_{1/2}$ = 0.80 V). The lack of the limiting current plateau could be due to a nonuniform distribution of electrocatalytic sites.[32] The number ($n$) of transfer electrons per $O_2$ involved in ORR is 3.6, manifesting a dominant four-electron process (Figure S12). To further evaluate the ORR pathways for the catalyst investigated in this study, we performed rotating ring-disk electrode (RRDE) measurements. As shown in Figure 4c, BClCNTs exhibit high disk current densities (~6 mA $cm^{-2}$) for $O_2$ reduction and extremely low ring current densities (~5 × $10^{-4}$ mA $cm^{-2}$) for peroxide oxidation. Moreover, a small ratio of peroxide species (less than 2%) is obtained in the potential range from 0.2 to 0.8 V (Figure 4d). The ORR activity of as-synthesized BClCNTs is superior to the other resultant products (Figure S13) and comparable to/even in excess of most of HFCNTs-based ORR catalysts (Figure 4e).[10,12,19,20] The excellent ORR activity can be mainly



DOI: 10.1021/acsenergylett.7b01133
ACS Energy Lett. 2018, 3, 184−190

attributed to the synergetic role of B and Cl atoms in the BClCNTs, as disclosed by the above-mentioned theoretical calculations. In addition, the Nyquist plots obtained were modeled and interpreted in terms of an appropriate electric equivalent circuit (Figure S14). The detailed view of Nyquist plots presents a lower internal resistance ($R_\Omega$) and a much lower charge transfer resistance ($R_{ct}$) for BClCNTs-2, suggesting the enhanced conductivity and the fast kinetic process for BClCNTs-2.

After 10000 continuous cycles, $E_{1/2}$ of BClCNTs-2 exhibits a slightly negative shift of 2 mV (Figure 4f), which outstrips most non-noble metal catalysts along with Pt/C catalysts (13 mV, inset image of Figure 4f).[10,33] To distinguish the possible effect of $O_2$ molecules,[34] we also measured the current response of the BClCNTs-2 for 10000 s against the $O_2$ atmosphere (Figure S15). As a reference point, the corresponding current−time ($i$−$t$) chronoamperometric response for a Pt/C electrode presents a quick 26% current drop (inset image of Figure S15) under the same conditions against only 7% of our BClCNTs-2. BClCNTs also endow good tolerance to the crossover effect of methanol oxidation and CO poisoning (Figure S16). The high degree of graphitization and the robust 1D microstructure of CNTs could be responsible for the high durability of the BClCNTs electrocatalyst.[32]

In summary, we first convert 2D boron carbide nanoflakes into BClCNTs via a simple chemical tailoring technique with $Cl_2$. By choosing different chlorine-to-carbide molar ratios, the doping configurations of B and Cl can be facilely controlled. As expected, BClCNTs present excellent ORR performance, which is due to possible synergetic effects between electron acceptor (B) and electron donor (Cl) atoms. The findings in this study could pave the way for industrial-level applications of heteroatom-doped CNTs.

## ■ ASSOCIATED CONTENT

### Supporting Information

The Supporting Information is available free of charge on the ACS Publications website at DOI: 10.1021/acsenergylett.7b01133.

Experimental methods, Figures S1−S16, showing the total energy as a function of optimization and equilibirum geometries, NBO charges, HOMO and LUMO spatial distributions, SEM images, XRD patterns, illustration of fabrication procedures, TEM images, Raman spectra, XPS spectra, transferred electron numbers and LSV curves, ORR activity, EIS, $i$−$t$ chronoamperometric response, and methanol tolerance and CO poisoning, Tables S1−S4, showing input coordinates, electronic properties, XPS elemental distribution, comparison of catalytic parameters, and refs S1−S17 (PDF)

## ■ AUTHOR INFORMATION


### Corresponding Author

*E-mail: msc@whut.edu.cn.

### ORCID

Daping He: 0000-0002-0284-4990

Shichun Mu: 0000-0003-3902-0976


### Notes

The authors declare no competing financial interest.

## ■ ACKNOWLEDGMENTS

We acknowledge support from the National Natural Science Foundation of China (NSFC) through Award No. 51672204 and No. 51372186. We express heartfelt thanks to Prof. Gaoke Zhang for the supply of computational resources in the School of Resources and Environmental Engineering, Wuhan University of Technology. We wish to thank Associate Prof. Xiaoqing Liu and Dr. Tingting Luo for TEM analytical measurements performed at JEM-2100F in the Materials Analysis Center of Wuhan University of Technology.

## ■ REFERENCES


(1) Iijima, S. Helical Microtubules of Graphitic Carbon. *Nature* **1991**, *354*, 56−59.

(2) Zhao, Y.; Yang, L.; Chen, S.; Wang, X.; Ma, Y.; Wu, Q.; Jiang, Y.; Qian, W.; Hu, Z. Can Boron and Nitrogen Co-Doping Improve Oxygen Reduction Reaction Activity of Carbon Nanotubes? *J. Am. Chem. Soc.* **2013**, *135*, 1201−1204.

(3) Guo, D.; Shibuya, R.; Akiba, C.; Saji, S.; Kondo, T.; Nakamura, J. Active Sites of Nitrogen-Doped Carbon Materials for Oxygen Reduction Reaction Clarified Using Model Catalysts. *Science* **2016**, *351*, 361−365.

(4) Chen, Z.; Higgins, D.; Yu, A.; Zhang, L.; Zhang, J. A Review on Non-Precious Metal Electrocatalysts for PEM Fuel Cells. *Energy Environ. Sci.* **2011**, *4*, 3167−3192.

(5) Feng, N.; He, P.; Zhou, H. Critical Challenges in Rechargeable Aprotic Li-$O_2$ Batteries. *Adv. Energy Mater.* **2016**, *6*, 1502303.

(6) Wang, S.; Yu, D.; Dai, L. Polyelectrolyte Functionalized Carbon Nanotubes as Efficient Metal-free Electrocatalysts for Oxygen Reduction. *J. Am. Chem. Soc.* **2011**, *133*, 5182−5185.

(7) Yang, L.; Jiang, S.; Zhao, Y.; Zhu, L.; Chen, S.; Wang, X.; Wu, Q.; Ma, J.; Ma, Y.; Hu, Z. Boron-doped Carbon Nanotubes as Metal-Free Electrocatalysts for the Oxygen Reduction Reaction. *Angew. Chem.* **2011**, *123*, 7270−7273; *Angew. Chem., Int. Ed.* **2011**, *50*, 7132−7135.

(8) Gong, K.; Du, F.; Xia, Z.; Durstock, M.; Dai, L. Nitrogen-Doped Carbon Nanotube Arrays with High Electrocatalytic Activity for Oxygen Reduction. *Science* **2009**, *323*, 760−764.

(9) Yang, J.; Sun, H.; Liang, H.; Ji, H.; Song, L.; Gao, C.; Xu, H. A Highly Efficient Metal-Free Oxygen Reduction Electrocatalyst Assembled from Carbon Nanotubes and Graphene. *Adv. Mater.* **2016**, *28*, 4606−4613.

(10) Chen, S.; Bi, J.; Zhao, Y.; Yang, L.; Zhang, C.; Ma, Y.; Wu, Q.; Wang, X.; Hu, Z. Nitrogen-Doped Carbon Nanocages as Efficient Metal-Free Electrocatalysts for Oxygen Reduction Reaction. *Adv. Mater.* **2012**, *24*, 5593−5597.

(11) Liu, H.; Sun, P.; Feng, M.; Liu, H.; Yang, S.; Wang, L.; Wang, Z. Nitrogen and Sulfur Co-Doped CNT-COOH as An Efficient Metal-Free Catalyst for the Degradation of UV Filter BP-4 Based on Sulfate Radicals. *Appl. Catal., B* **2016**, *187*, 1−10.

(12) Wang, S.; Iyyamperumal, E.; Roy, A.; Xue, Y.; Yu, D.; Dai, L. Vertically Aligned BCN Nanotubes as Efficient Metal-Free Electrocatalysts for the Oxygen Reduction Reaction: a Synergetic Effect by Co-Doping with Boron and Nitrogen. *Angew. Chem.* **2011**, *123*, 11960−11964; *Angew. Chem., Int. Ed.* **2011**, *50*, 11756−11760.

(13) Cho, W. S.; Hamada, E.; Kondo, Y.; Takayanagi, K. Synthesis of Carbon Nanotubes from Bulk Polymer. *Appl. Phys. Lett.* **1996**, *69*, 278.

(14) Hsu, W. K.; Terrones, M.; Hare, J. P.; Terrones, H.; Kroto, H. W.; Walton, D. R. M. Electrolytic Formation of Carbon Nanostructures. *Chem. Phys. Lett.* **1996**, *262*, 161−166.

(15) Kyotani, T.; Tsai, L-f.; Tomita, A. Preparation of Ultrafine Carbon Tubes in Nanochannels of An Anodic Aluminum Oxide Film. *Chem. Mater.* **1996**, *8*, 2109−2113.

(16) Meng, J.; Niu, C.; Xu, L.; Li, J.; Liu, X.; Wang, X.; Wu, Y.; Xu, X.; Chen, W.; Li, Q.; et al. General Oriented Formation of Carbon




DOI: 10.1021/acsenergylett.7b01133
*ACS Energy Lett.* 2018, 3, 184−190

Nanotubes from Metal-Organic Frameworks. *J. Am. Chem. Soc.* **2017**, *139*, 8212−8221.
(17) Li, L.; Dai, P.; Gu, X.; Wang, Y.; Yan, L.; Zhao, X. High Oxygen Reduction Activity On a Metal-Organic Framework Derived Carbon Combined with High Degree of Graphitization and Pyridinic-N dopants. *J. Mater. Chem. A* **2017**, *5*, 789−795.
(18) Guan, Y.; Yu, L.; Lou, X. W. Formation of Single-Holed Cobalt/N-Doped Carbon Hollow Particles with Enhanced Electrocatalytic Activity toward Oxygen Reduction Reaction in Alkaline Media. *Adv. Sci.* **2017**, *4*, 1700247.
(19) Guan, B. Y.; Yu, L.; Lou, X. W. D. A Dual-Metal-Organic-Framework Derived Electrocatalyst for Oxygen Reduction. *Energy Environ. Sci.* **2016**, *9*, 3092−3096.
(20) Zhang, Z.; Mu, S.; Zhang, B.; Tao, L.; Huang, S.; Huang, Y.; Gao, F.; Zhao, Y. A Novel Synthesis of Carbon Nanotubes Directly from an Indecomposable Solid Carbon Source for Electrochemical Applications. *J. Mater. Chem. A* **2016**, *4*, 2137−2146.
(21) Presser, V.; Heon, M.; Gogotsi, Y. Carbide-Derived Carbons-from Porous Networks to Nanotubes and Graphene. *Adv. Funct. Mater.* **2011**, *21*, 810−833.
(22) Kou, Z.; Meng, T.; Guo, B.; Amiinu, I. S.; Li, W.; Zhang, J.; Mu, S. A Generic Conversion Strategy: From 2D Metal Carbides ($M_xC_y$) to M-self-doped Graphene toward High-efficiency Energy Applications. *Adv. Funct. Mater.* **2017**, *27*, 1604904.
(23) Grujicic, M.; Cao, G.; Rao, A. M.; Tritt, T. M.; Nayak, S. UV-light Enhanced Oxidation of Carbon Nanotubes. *Appl. Surf. Sci.* **2003**, *214*, 289−303.
(24) Zhang, L.; Xia, Z. Mechanisms of Oxygen Reduction Reaction on Nitrogen-Doped Graphene for Fuel Cells. *J. Phys. Chem. C* **2011**, *115*, 11170−11176.
(25) Khalfoun, H.; Hermet, P.; Henrard, L.; Latil, S. B and N Codoping Effect on Electronic Transport in Carbon Nanotubes. *Phys. Rev. B: Condens. Matter Mater. Phys.* **2010**, *81*, 193411.
(26) Lazzari, R.; Vast, N.; Besson, J.; Baroni, S.; Dal Corso, A. Atomic Structure and Vibrational Properties of Icosahedral $B_4C$ Boron Carbide. *Phys. Rev. Lett.* **1999**, *83*, 3230−3233.
(27) Ferrari, A. C.; Basko, D. M. Raman Spectroscopy as a Versatile Tool for Studying the Properties of Graphene. *Nat. Nanotechnol.* **2013**, *8*, 235−246.
(28) Hendrickson, D. N.; Hollander, J. M.; Jolly, W. L. Core-Electron Binding Energies for Compounds of Boron, Carbon, and Chromium. *Inorg. Chem.* **1970**, *9*, 612−615.
(29) Li, X.; Lau, S. P.; Tang, L.; Ji, R.; Yang, P. Multicolour Light Emission from Chlorine-Doped Graphene Quantum Dots. *J. Mater. Chem. C* **2013**, *1*, 7308−7313.
(30) Chen, W.; Roberts, J. T. Surface Chemistry of $TiCl_4$ on W (100). *Surf. Sci.* **1996**, *359*, 93−106.
(31) Kim, E.; Oh, I.; Kwak, J. Local Atomic and Electronic Structure of Boron Chemical Doping in Monolayer Graphene. *Electrochem. Commun.* **2001**, *3*, 608−612.
(32) Jiang, R.; Anson, F. C. The Origin of Inclined Plateau Currents in Steady-State Voltammograms for Electrode Processes Involving Electrocatalysis. *J. Electroanal. Chem. Interfacial Electrochem.* **1991**, *305*, 171−184.
(33) Li, Y.; Zhou, W.; Wang, H.; Xie, L.; Liang, Y.; Wei, F.; Idrobo, J.-C.; Pennycook, S. J.; Dai, H. An Oxygen Reduction Electrocatalyst Based on Carbon Nanotube-Graphene Complexes. *Nat. Nanotechnol.* **2012**, *7*, 394−400.
(34) Yang, H.; Miao, J.; Hung, S.; Chen, J.; Tao, H.; Wang, X.; Zhang, L.; Chen, R.; Gao, J.; Chen, H.; et al. Identification of Catalytic Sites for Oxygen Reduction and Oxygen Evolution in N-doped Graphene Materials: Development of Highly Efficient Metal-Free Bifunctional Electrocatalyst. *Sci. Adv.* **2016**, *2*, e1501122.



DOI: 10.1021/acsenergylett.7b01133
*ACS Energy Lett.* 2018, 3, 184−190